Journal of Power Sources 256 (2014) 125–132

Contents lists available at ScienceDirect

Journal of Power Sources

journal homepage: www.elsevier.com/locate/jpowsour

Controllable synthesis of vertically aligned polypyrrole nanowires as advanced electrode support for fuel cells

Zhangxun Xia [a,b], Suli Wang [a], Luhua Jiang [a], Hai Sun [a], Gongquan Sun [a,*]

[a] Division of Fuel Cell & Battery, Dalian National Laboratory for Clean Energy, Dalian Institute of Chemical Physics, Chinese Academy of Sciences, Dalian, China

[b] University of Chinese Academy of Sciences, Beijing, China

HIGHLIGHTS

- The morphology of the PPy nanowires grown on Pd modified Nafion® membranes can be controlled.
- The hydrophobicity/hydrophilicity of the PPy nanowires is related with the morphology.
- The enhancement of catalyst utilization is observed with the application of the PPy nanowires as cathode support in DMFCs.
- The most ordered PPy as the support of cathode for DMFCs displays the best performance due to the facile mass transport.

ARTICLE INFO

Article history:
Received 29 August 2013
Received in revised form
30 November 2013
Accepted 2 December 2013
Available online 13 December 2013

Keywords:
Fuel cells
Polypyrrole
Nanowires
Electrochemical polymerization

ABSTRACT

Here, we develop a facile electrochemical polymerization method for the synthesis of polypyrrole (PPy) nanowires on Pd modified Nafion® membranes. Interestingly, with altering the deposition potential and temperature, we can easily tune the PPy nanowires from disordered nanostructures to well ordered vertically aligned nanowires. The various PPy nanowires show similar electronic conductivity but diverse hydrophobicity/hydrophilicity. The ordered PPy nanowires can significantly facilitate the mass transport and enhance the catalyst utilization. These two factors together make an obvious performance improvement of fuel cells.

1. Introduction

Polymer electrolyte membrane fuel cell (PEMFC), which converts chemical energy directly to electricity, is one of the most promising clean energy technologies attracting great research interests from 1990s. [1–4] Membrane electrode assembly (MEA), as the key component of fuel cells, acts as a complicated system which involves transports of both liquid and gaseous reactants/products. Thus performance of fuel cells significantly depends on the microstructure of the electrode, i.e., tailoring the micro- and macro-structure of the cathodic electrode can largely improve the oxygen and water transports. [5–7] Traditional electrodes with disordered microstructures lead to both poor mass transport of reactants/products and low utilization of catalyst, which has already become a major bottleneck for further enhancement of fuel cell performances.

Ordered-structured MEA, proposed by Middelman as early as 2002, [8] in which the electronic conductor loaded with catalysts and proton conductors coated outside orientates perpendicularly to the membrane, is supposed to be able to maximize the utilization of catalyst and greatly enhance the mass transport of reactants/products and electrons/protons. Recently, MEAs with ordered nanostructures have been developed based on various materials, such as carbon nanotube arrays, organic crystalloid whiskers and conductive polymer nanowire arrays. [9–15] However, to our knowledge, the fabrication of such ordered-structured materials as MEAs is still far from facility. Our previous paper reports a facile fabrication of vertically oriented polypyrrole (PPy) nanowire arrays on modified Nafion® membranes *via* electrochemical polymerization, which is confirmed a promising electrode material for direct methanol fuel cells (DMFCs). [16] However, the growth mechanism and the morphological controllability of the ordered PPy are still undiscovered.

* Corresponding author. Tel./fax: +86 411 84379063.
E-mail address: gqsun@dicp.ac.cn (G. Sun).

0378-7753/$ – see front matter © 2013 Elsevier B.V. All rights reserved.
http://dx.doi.org/10.1016/j.jpowsour.2013.12.013

In this work, facile approaches to control the morphology of the PPy nanowires are put forward and the growth mechanism of the PPy nanowires on Pd-modified Nafion® membranes is proposed. The properties, such as wetting behaviors and electronic conductivities, of the PPy nanowires with various morphologies are investigated. The PPy nanowires on Nafion® membranes as cathode supports are fabricated, and the dependence of DMFC performances on the morphologies of the PPy nanostructures is discussed.

2. Experimental

2.1. Preparation of the PPy nanowires on Pd/Nafion® membranes

The experimental details of modification of Nafion® membrane with Pd could be found in our previous work. [17] In brief, a piece of Nafion® 115 membrane (DuPont) was immersed in Pd activation solution, and then rinsed with de-ionized water. The membrane was then immersed in borane dimethylamine complex (97%, Alfa Aesar) solution (1 mg mL^{-1}, aq.) for 5 min. The as prepared Pd activated Nafion® 115 membrane was then immersed in Pd chemical plating solution (Palatec) at 52 °C for 20 min. The as-prepared Pd-modified Nafion® membrane was denoted as Pd/Nafion®.

The PPy nanowires were prepared *via* electrochemical polymerization controlled by an electrochemical workstation (SI1287, Solartron Co.). The Pd/Nafion® membrane sealed by a plastic holder with Pt wire as electron conductor contacting with Pd membrane was used as the working electrode. A Pt plate (5 × 7 cm^2) and a saturated calomel electrode (SCE) were used as the counter and reference electrode, respectively. The electrolyte solution for electrochemical polymerization was prepared as follows: 15.406 g disodium hydrogen phosphate dodecahydrate ($Na_2HPO_4{\cdot}12H_2O$, 99%, Tianjin Damao Reagent) and 6.240 g monosodium phosphate dihydrate ($NaH_2PO_4{\cdot}2H_2O$, 99%, Tianjin Damao Reagent) were dissolved in 200 mL de-ionized water to prepare 0.2 M phosphate buffer solution (PBS); 3.884 g *p*-toluenesulfonyl sodium (98.5%, Tianjin Guangfu Reagent) was then dissolved in 200 mL PBS; 1.388 mL pyrrole (98%, Sinopharm Chemical Reagent) was dispersed in the above solution by ultrasonication. The electrochemical polymerization of pyrrole was realized by applying a constant potential, e.g., 0.60, 0.65, 0.70, 0.75, 0.80 and 0.85 V *vs.* SCE on the working electrodes for 1800s at 278 K. The obtained PPy nanowires on Pd/Nafion® samples were denoted as PPy-E60, PPy-E65, PPy-E70, PPy-E75, PPy-E80 and PPy-E85, respectively. To study the effect of the electrolyte temperature on the morphology, the temperature was kept at 278, 298 and 318 K while the potential applied on the working electrode was controlled at 0.65 V *vs.* SCE. Accordingly, the obtained samples were denoted as PPy-T278, PPy-T298 and PPy-T318, respectively.

2.2. Fabrication of MEAs

To investigate the effect of the PPy nanowire morphologies on performance of DMFCs, the MEAs with different PPy samples applied as cathodes were fabricated as follows. By spraying catalyst ink composed of commercial Pt black (Johnson Matthey Co.) on the PPy nanowires, the cathode with a Pt loading of 0.5 mg cm^{-2} was obtained. By brushing catalyst ink composed of a commercial 60 wt.% PtRu/C (Johnson Matthey Co.) on the gas diffusion layer (GDL), the anode with a PtRu loading of 3.6 mg cm^{-2} was obtained. The MEAs with an active area of 2 × 2 cm^2 was fabricated by hot pressing the catalyst coated membrane of cathode sandwiched between the anode and the cathode gas diffusion layer at 120 °C and 200 kg cm^{-2} for 1 min. The MEAs with PPy nanostructures of PPy-E65, PPy-E75 and PPy-E85 applied to the cathode were denoted as MEA-E65, MEA-E75 and MEA-E85, respectively. For comparison, the traditional MEA with pristine Nafion® 115 membrane was denoted as MEA-T.

2.3. Characterization of the PPy nanowires on Pd/Nafion®

The morphologies of the PPy nanowire samples were investigated by field emission scanning electron microscope (FESEM, S-4800, Hitachi) and transmission electron microscope (TEM, JEM-2011EM, JEOL). The wetting behaviors of the PPy layers were measured by a contact-angle meter (JC2000C1, Shanghai Powereach), and the sheet resistances of the surfaces were characterized by a four point probe measurement (SZ-82, Suzhou Telecommunication).

2.4. DMFC Single cell performance tests

The CV curves of cathode were recorded by an electrochemical workstation (SI1287 and SI1260, Solartron Co.) at 80 °C. The cathode fed with de-ionized water at a flow rate of 1 mL min^{-1} is used as the working electrode and the anode fed with hydrogen at a flow rate of 50 mL min^{-1} used as both reference and counter electrode. The scan rate is 20 mV s^{-1}. The anode polarization curves were recorded by the electrochemical workstation (SI1287 and SI1260, Solartron Co.) at 80 °C. The anode fed with 0.5 M methanol solution at a flow rate of 1 mL min^{-1} is used as the working electrode and the cathode fed with hydrogen at a flow rate of 50 mL min^{-1} is used as both reference and counter electrode. The scan rate is 2 mV s^{-1}. The discharging curves (*I*–*V*) of DMFCs were evaluated by a fuel cell test system (FCTS, Arbin Co.) under an oxygen back pressure of 0.2 MPa and methanol concentration of 0.5 M. The working temperature of the single cells is 80 °C. The flow rates of oxygen and methanol solution is 80 mL min^{-1} and 1 mL min^{-1}, respectively. The oxygen gain of DMFCs was the difference of the cell voltages at the same current density when the cathode was fed with oxygen or air (without back pressures).

3. Results and discussion

3.1. Controllable growth of the PPy nanowires

To understand the growth processes of the PPy nanowires over Pd/Nafion® membranes, a typical chronoamperometric curve

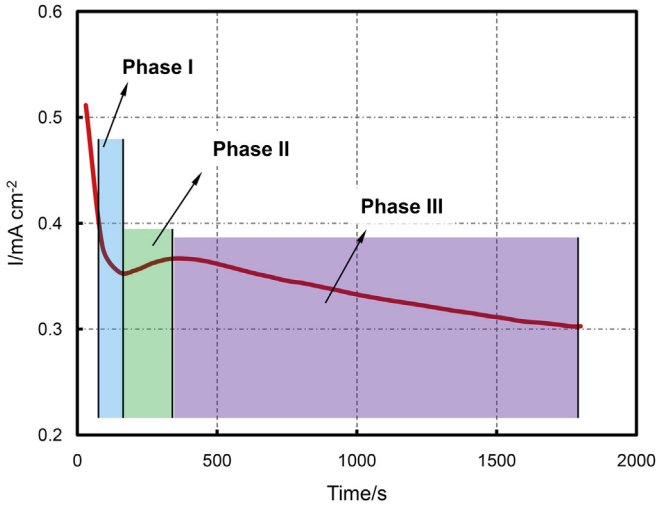

Fig. 1. A typical chronoamperometric curve of the synthesis of the PPy nanowires.

during the electrochemical polymerization of pyrrole (sample PPy-E65) is collected, as shown in Fig. 1, and analyzed. Considering that the polymerization of pyrrole in general consists of two major steps: nucleation and oriented growth, [18–24] the chronoamperometric curve is divided into three phases based on the turning points of current, ignoring the initial seconds with a sharp decrease in current due to double-layer charge/discharge: phase I, a relatively moderate decrease in currents following the double-layer charge/discharge period standing for the initial electro-oxidation of pyrrole molecules; phase II, a slow rise in currents from the trough to the followed peak, suggesting a gradually growing rate of pyrrole polymerization; phase III, a quasi-stable phase from the current peak to the ending point, possibly standing for a steady electrochemical polymerization process of pyrrole. The integrated charges for phase II and III might be crucially interrelated with the shape of the PPy nanowires.

Fig. 2a–f is the SEM images of the PPy nanowires obtained at different polymerization potentials. The polymerization potentials are chosen based on the cyclic voltammogram (CV) curves of pyrrole electrochemical polymerization (see Fig. S1). It is clear that the

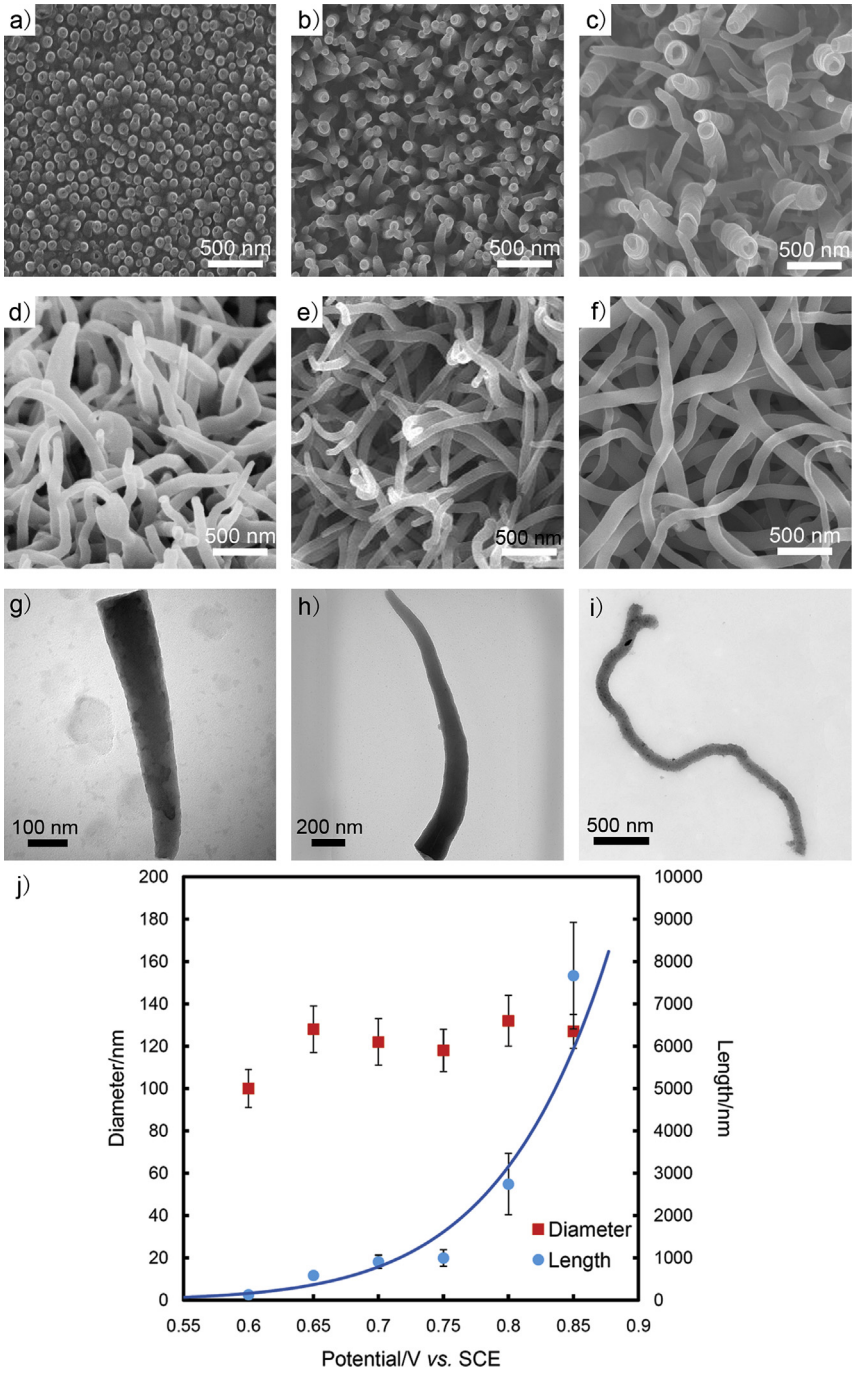

Fig. 2. Morphologies of the PPy nanowires polymerized at different potentials. a–f, SEM images in top views of PPy-E60, PPy-E65, PPy-E70, PPy-E75, PPy-E80 and PPy-E85, respectively; g–i, TEM images of the typical PPy nanowires obtained from PPy-E65, PPy-E75, and PPy-E85, respectively; j, variation of the average diameters/lengths of PPy at different polymerization potentials; polymerization temperature is 298 K.

morphology of the PPy nanostructures changes significantly with polymerization potentials. The PPy formed at a relatively low potential ($E = 0.6$ V *vs.* SCE) tends to form a vertically aligned nanorods (Fig. 2a). As the potential increases from 0.6 to 0.85 V *vs.* SCE, the morphology of PPy changes from nanorods to the vertically aligned nanowires (Fig. 1b and c), and finally to disordered nanofibers (Fig. 2e and f). To further investigate the morphological details of the PPy nanowires, TEM images are shown in Fig. 2g–i. The average length of the nanowires exponentially increases with the rise of the polymerization potential, while the average diameter changes unnoticeably, as shown in Fig. 2j.

The influence of polymerization temperatures on the PPy nanowire morphology is different from that of potentials. As shown in Fig. 3a–c, both the length and diameter of the PPy nanowires increase with the temperature rising from 278 K to 318 K, while the structure of the PPy nanowire arrays also changes from orderliness to disorderliness. The temperature dependence of the average length and diameter of the PPy is quantitatively shown in Fig. 3d. The related mechanism is discussed in next paragraph combined with the integrated charges during the PPy formation mentioned above.

The chronoamperometric curves under different potentials and temperatures are shown in Fig. S2, and divided into the three phases mentioned above *via* asterisks. The quasi-stable currents at the end of 1800s increase with the rise of potential applied, which is reasonable considering that the electrochemical reaction should be accelerated exponentially according to Butler–Volmer equation. [25–27] The currents increase moderately along with the increase in temperature of the electrolyte solution as exhibited in Fig. S2b.The variation of the integrated charges for phase II (Q_{II}) and phase III (Q_{III}) with potentials and temperatures are plotted in Fig. 4b and c, respectively. As shown in Fig. 4a, Q_{II} at different polymerization potentials stays almost constant, while Q_{III} increases sharply with the rise of the potentials. Furthermore, the variation of Q_{II} and Q_{III} with the polymerization temperatures, as shown in Fig. 4b, follows a similar trend of a remarkable increase. It is found that the variational trends of Q_{II} and Q_{III} with the potentials follow similar trendlines of the PPy diameters and lengths with potentials in Fig. 2j. Also the variational trends of Q_{II} and Q_{III} with temperatures follow that of PPy diameters and lengths with temperatures in Fig. 3d. Drawing from these phenomenon, we can deduce that phase II is related with PPy diameter and phase III with PPy length, that is, phase II corresponds to the nucleation process, in which the moderate increase of current should be explained as the expanding of the PPy nucleus, and phase III to the PPy growth process. Informed by numerous literature [28–30], in the nucleation period, because of the existence of *p*-toluenesulfonyl sodium as "soft template", the interaction between the anions and pyrrole molecules (or PPy oligomers) aggravates the polarization of PPy electrochemical polymerization. Hence, the electrochemically active sites, such as nano-defects or nano-particles, could be the nucleation sites of PPy growth. This process of nucleation could be critical for diameters of the PPy nanowires, which is largely influenced by temperature rather than potential. Further, the process of PPy vertical growth should be determinative for lengths of the PPy nanowires. The quasi-stable current in this period could be the result of the constant growth rate, which is obviously accelerated by the rise in potentials and temperatures. The electrochemical polymerization processes discussed above are summarized in Scheme 1.

3.2. Water wetting behaviors and electronic conductivities of the PPy nanowires

The mass transport of gas and liquid at cathode and anode is remarkably related to the hydrophilicity and hydrophobicity of the

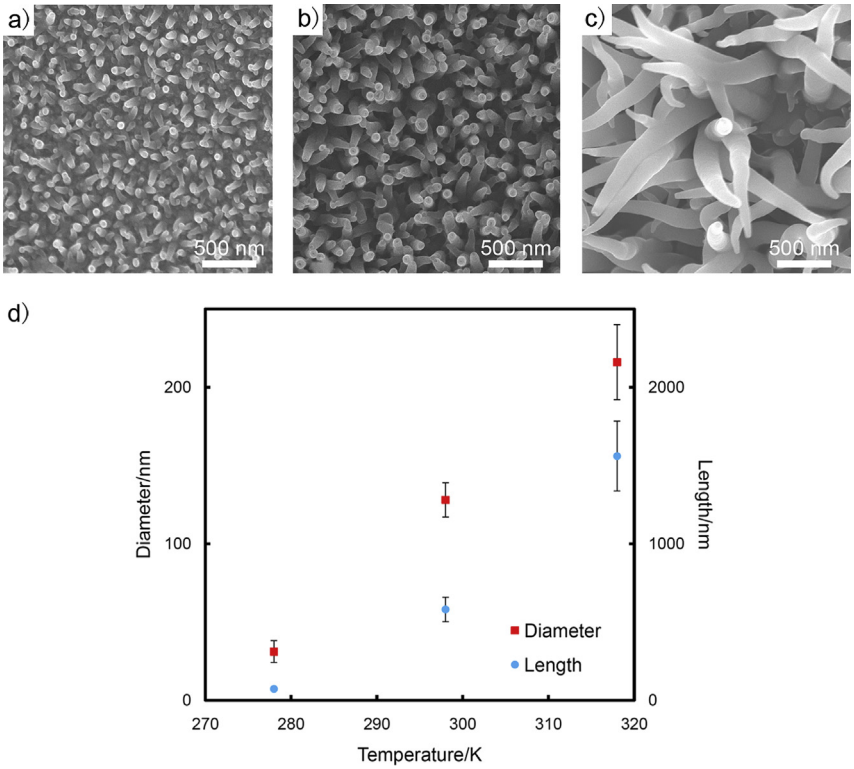

Fig. 3. Morphologies of the PPy nanowires polymerized at different temperatures. a–c, SEM images in top views of PPy-T278, PPy-T298 and PPy-T318, respectively; d, the variation of the average diameters/lengths of PPy at different polymerization temperatures; polymerization potential is 0.65 V *vs.* SCE.

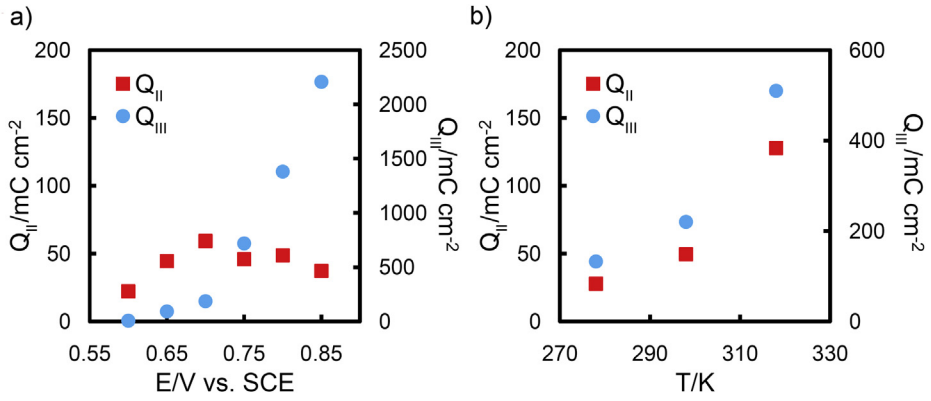

Fig. 4. Coulombic study of electrochemical polymerization processes of the PPy nanowires. a, Variation of Q_{II} and Q_{III} with polymerization potentials; b, variation of Q_{II} and Q_{III} with polymerization temperatures.

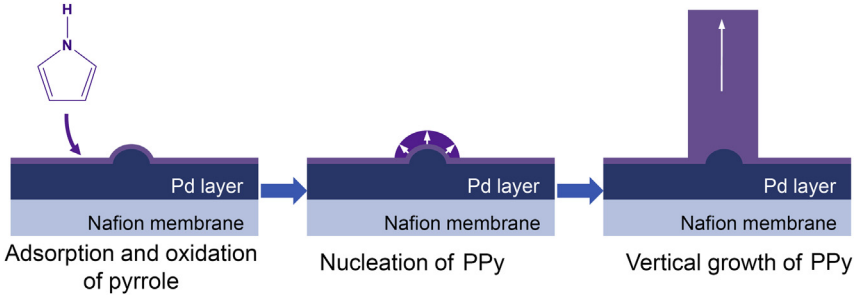

Scheme 1. Scheme for the electrochemical growth process of the PPy nanowires.

electrodes. [31] Hence, to obtain materials with proper wetting properties is crucial for DMFCs. Fig. 5a–d reveals a dramatic variation of wetting behaviors of water on the PPy nanowires with different morphologies. A volcano-like curve is obtained by correlating the contact angles (CAs) and polymerization potentials as shown in Fig. 5e. The PPy with a morphology of short rod arrays (PPy-E60, Fig. 2a) shows a moderate hydrophobicity (CA = 92.5°), while as the applied potential increases, CA rises to 132° (PPy-E65, Fig. 2b) and 125° (PPy-E70, Fig. 2c) with the PPy morphology changing from short rod arrays to vertically aligned nanowire arrays. Further increasing the potentials applied to the substrate, CA drops significantly. At the potential as high as 0.85 V (PPy-E85),

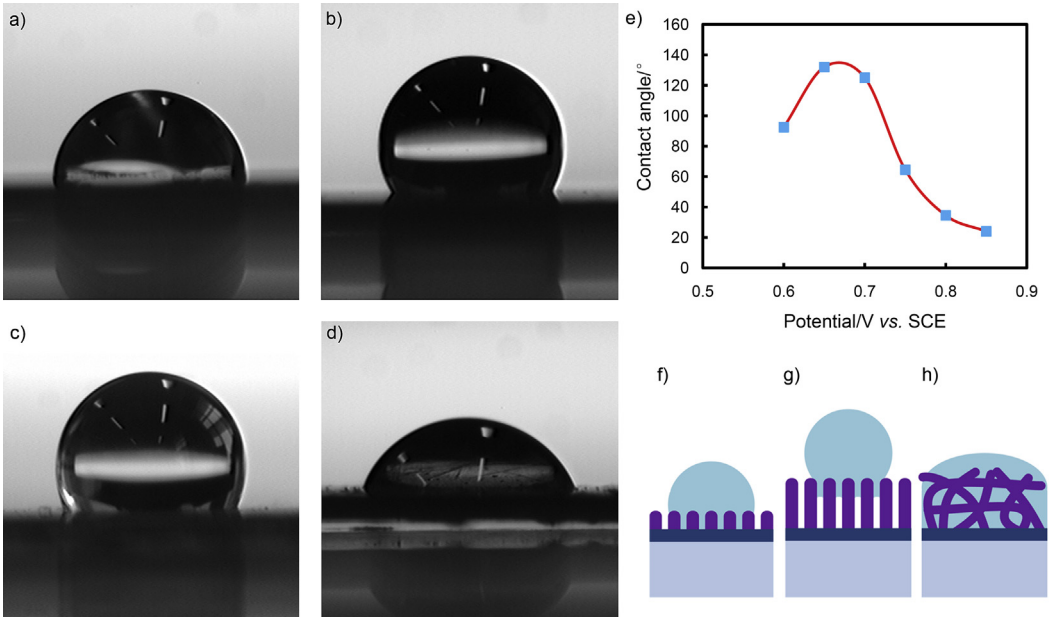

Fig. 5. Wetting behaviors of water on the surfaces of the PPy nanostructures. a–d, digital photos of wetting behaviors of water for samples of PPy-E60, PPy-E65, PPy-E70 and PPy-E75; e, relation curve for water contact angles and polymerization potentials; f–h, schemes of water wetting behaviors on PPy nanostructures with different morphologies.

the PPy with morphology of nanowire network (Fig. 2f) is totally hydrophilic (CA = 18°).

The variation of CA is probably related with the surface morphologies as illustrated in Fig. 5f–h [32,33]. For the case of short PPy rod arrays corresponding to Fig. 5a, the wetting behavior is proposed following the Wenzel model as shown in Fig. 5f [34]. The water droplet follows the contours of this type of surface. Thus the increase of surface roughness expands the real area of contact surface, and consequently enlarges CA. For the case of vertically aligned PPy nanowire arrays corresponding to Fig. 4b and c, the wetting behavior is proposed following the Cassie–Baxter model as shown in Fig. 5g [35], in which the droplet is energetically favorable to bridge across the tops of the nanowires to form air gaps between the droplet and the flat surface. The second model can result in a greater CA compared with that of the first one for the air gaps formed between the interface. When it comes to the case of nanowire networks corresponding to Fig. 5d, following the model shown in Fig. 5h, the water droplet might permeate into the large gaps and contiguous pores formed within the orderless nanowire networks. Hence, the capillary effect renders the liquid dispersing among the layer of nanowire networks, and CA drops consequently.

Electronic conductivity of electrode materials is another critical issue that affects fuel cell performance greatly. The data showed in Fig. S3 are the electronic conductivities for different samples tested by a four-probe method. Although both the thicknesses and the morphologies of the PPy nanowires are different, the results from the four point probe measurement could provide an approximate conductivity value of the layer. As plotted in Fig. S3, the electronic conductivities for the PPy nanowires with different morphologies are in the same magnitude ($10–10^2$ S cm^{-1}). Despite the electronic conductivity of the PPy wires is one order of magnitude lower than that of carbon materials (such as Vulcan XC-72) commonly used in fuel cells, the ohmic resistances, obtained from the real axis intercepts of the electrochemical impedance spectra (EIS) curves (Fig. S4), of DMFCs (MEA-E65, MEA-E75 and MEA-E85) are not increased noticeably compared to that without PPy as catalyst supports (MEA-T), as shown in Table 1.

3.3. DMFC Performances of MEAs with the PPy nanowires

To further investigate the effect of PPy nanostructures as the electrode support on DMFC performances, commercial Pt catalyst powder is sprayed on the PPy nanostructures with different morphologies to act as the cathode of DMFCs. A DMFC with a traditional cathode by dispersing Pt black directly on the Nafion 115 membrane is used for comparison. Fig. 6 is DMFC polarization curves and the power density curves. Apparently, the MEA with the most ordered PPy nanowire arrays (MEA-E65) exhibits the best performance with a peak power density of 98.2 mW cm^{-2}. With the sample of more disordered PPy nanowire arrays (MEA-E75), DMFC performance drops (peak power density is 72.4 mW cm^{-2}) apparently, while DMFC with the least ordered PPy nanostructure (MEA-E85) shows the lowest performance (peak power density is 60.5 mW cm^{-2}). Compared with the traditional electrode (MEA-T), the novel electrodes with PPy nanoarrays display apparently

Table 1
Electrochemical characteristics of DMFCs.

MEA samples	Peak power density/ mW cm^{-2}	ECSA/m^2 g$^{-1}_{Pt}$	Ohmic resistance/ Ω cm^2
MEA-E65	98.2	25.77	0.259
MEA-E75	72.4	28.40	0.314
MEA-E85	60.5	28.86	0.357
MEA-T	66.8	16.71	0.262

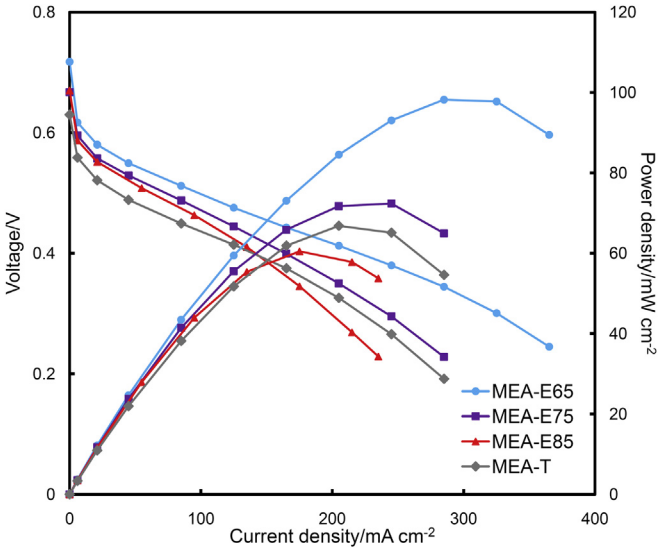

Fig. 6. Polarization curves and power density curves for DMFCs with MEA-E65 (circle), MEA-E75 (square), MEA-E85 (triangle) and MEA-T (diamond); the cell temperature is 80 °C; flow rates of methanol solution (0.5 M aq.) and oxygen (0.2 MPa back pressure) at 1 mL min^{-1} and 80 mL min^{-1}, respectively.

superior activity in the low current density region (typically lower than 150 mA cm^{-2}), i.e., the electrochemical activation controlled region. To further understanding the effects of the PPy nanowires applied as the cathode supports in DMFCs, the cathode polarization curves are obtained by adding the anode polarization curves to DMFC polarization curves, as shown in Fig. 7. The three PPy nanostructure-supported catalyst layers show similar cathode polarizations of the electrochemical activation region, obviously less than that of the traditional electrode. The improvement in the activation region for the novel electrodes suggests a higher utilization of Pt in the cathode with the PPy supports, which is evidenced by the larger electrochemical surface area (ECSA, listed in Table 1) calculated from the background CVs (Fig. 8) by assuming

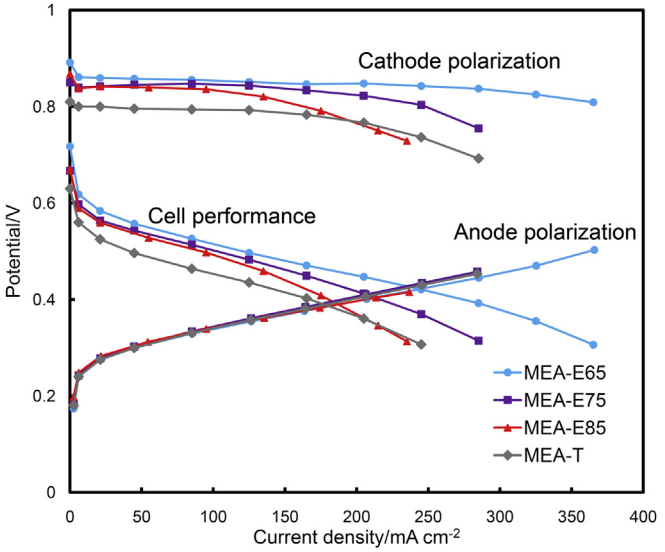

Fig. 7. IR-corrected polarization curves for DMFCs with MEA-E65 (circle), MEA-E75 (square), MEA-E85 (triangle) and MEA-T (diamond); the cell temperature is 80 °C; flow rates of methanol solution (0.5 M aq.) and oxygen (0.2 MPa back pressure) at 1 mL min^{-1} and 80 mL min^{-1}, respectively.

that the electric charge for the H_{ad}/H_{des} is 0.210 mC cm^{-2}, [36] compared to the traditional cathode. The Pt utilization for the novel electrode is most likely enhanced by the porous structure of PPy supports.

For the mass transport dominated region (current density over 150 mA cm^{-2}), electrode performance is tightly related with the PPy morphologies, i.e., the cathode with PPy of the highest orderliness (MEA-E65) exhibits the best performance, followed by the less ordered electrode (MEA-E75), and the cathode with the most disordered and thickest PPy layer presents the worst performance. The mass transport in the cathodes is further investigated by analyzing the oxygen gain of the cathodes, which is defined as the differences of the potentials at a given current density when the cathode gas is changed from pure oxygen to air due to the reduced partial pressure of oxygen [37]. It is measured to evaluate the voltage loss caused by the insufficiency of oxygen transport. This parameter is crucially related to the structures of cathode in fuel cells when the operation conditions are identical. Fig. 9 exhibits the significant change in oxygen gain for the PPy nanowire electrode with different structures. It is clear that the best ordered cathode (MEA-E65) shows the lowest oxygen gain especially at the high current density, which further indicates that the microstructure of the electrode can facilitate the oxygen transport. The oxygen gain of MEA-E85 is even higher than that of the traditional cathode without PPy as support, which might be explained by that the performance loss caused by increased mass transport resistance conquers the benefit brought by the porous structure of the PPy nanowire arrays.

4. Conclusions

In summary, the morphologies and structures of the PPy nanowires on Pd/Nafion® can be controlled *via* altering potential and temperature during electrochemical polymerization processes of pyrrole. The diameter of the PPy nanowires is probably related with the nucleation process, while the length of the PPy nanowires is related with the oriented growth process. The morphological changes of the PPy nanostructures can greatly affect the hydrophilic/hydrophobic properties of the materials, but do not influence the electronic conductivities significantly. As a result, electrode performances are greatly affected by the structures of the PPy nanowires. The highest DMFC performance and the lowest oxygen gain for electrode constructed by the most ordered aligned PPy nanostructure indicating that the such ordered structures significantly enhance the mass transport of oxygen and water in the cathode. The elucidated mechanism of the PPy growth over Pd/Nafion® membranes and the proposed strategy to control the morphology of PPy in this work is expected to provide guidance for ordered nanostructured material preparation.

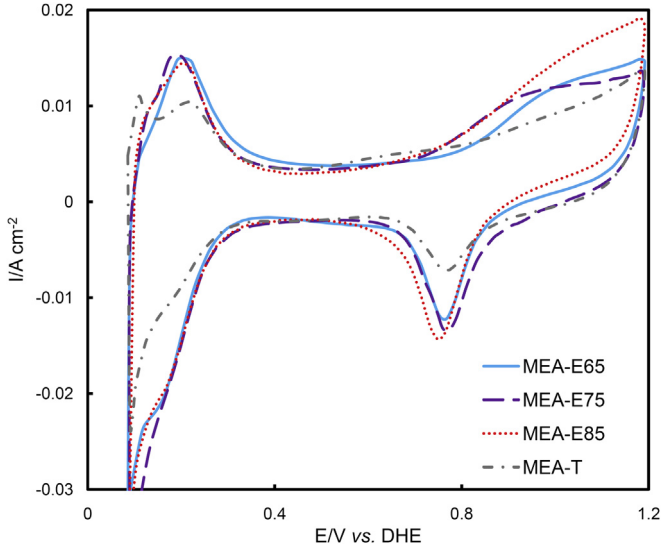

Fig. 8. Cathodic CV curves for the three DMFCs; the cell temperature is 80 °C; the scan rate is 50 mV s^{-1}.

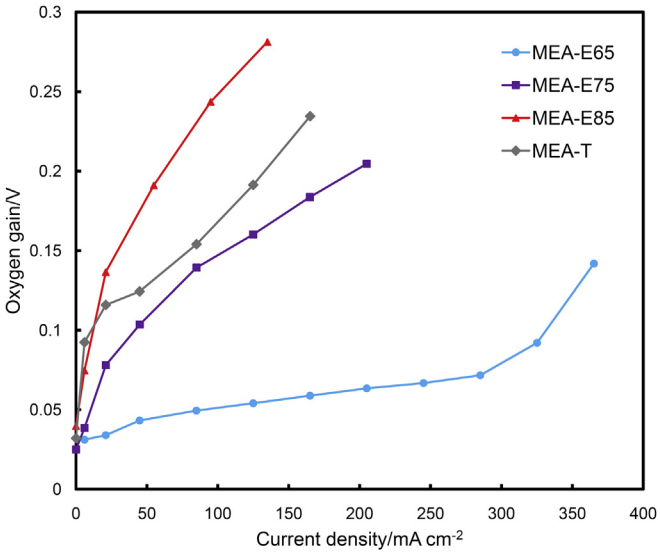

Fig. 9. Oxygen gain measured at 80 °C for DMFCs with MEA-E65 (circle), MEA-E75 (square), MEA-E85 (triangle) and MEA-T (diamond).

Acknowledgments

This work is financially supported by the National Basic Research Program of China (2012CB215500, 2011CB211706) and Chinese Academy of Sciences (61501070102B).

Appendix A. Supplementary data

Supplementary data related to this article can be found at http://dx.doi.org/10.1016/j.jpowsour.2013.12.013.

References

[1] B.C.H. Steele, A. Heinzel, Nature 414 (2001) 345.
[2] N.P. Brandon, S. Skinner, B.C.H. Steele, Annu. Rev. Mater. Res. 33 (2003) 183.
[3] C. Sealy, Mater. Today 11 (2008) 65.
[4] A.L. Dicks, J. Power Sources 156 (2006) 128.
[5] C.Y. Wang, Chem. Rev. 104 (2004) 4727.
[6] S. Um, C.Y. Wang, J. Power Sources 125 (2004) 40.
[7] K. Scott, W.M. Taama, P. Argyropoulos, K. Sundmacher, J. Power Sources 83 (1999) 204.
[8] E. Middelman, Fuel Cells Bull. 11 (2002) 9.
[9] W. Li, X. Wang, Z. Chen, M. Waje, Y. Yan, Langmuir 21 (2005) 9386.
[10] M.S. Saha, R. Li, X. Sun, J. Power Sources 177 (2008) 314.
[11] Z. Tian, S. Lim, C. Poh, Z. Tang, Z. Xia, Z. Luo, P. Shen, D. Chua, Y. Feng, Z. Shen, J. Lin, Adv. Energy Mater. 1 (2011) 1205.
[12] W. Zhang, A.I. Minett, M. Gao, J. Zhao, J.M. Razal, G.G. Wallace, T. Romeo, J. Chen, Adv. Energy Mater. 1 (2011) 671.
[13] M.K. Debe, A.K. Schmoeckel, S.M. Hendricks, G.D. Vernstrom, G.M. Haugen, R.T. Atanasoski, ECS Trans. 1 (2006) 51.
[14] M.K. Debe, A.K. Schmoeckel, G.D. Vernstrom, R. Atanasoski, J. Power Sources 161 (2006) 1002.
[15] L. Gancs, T. Kobayashi, M.K. Debe, R. Atanasoski, A. Wieckowski, Chem. Mater. 20 (2008) 2444.
[16] Z. Xia, S. Wang, Y. Li, L. Jiang, H. Sun, S. Zhu, D. Su, G. Sun, J. Mater. Chem. A 1 (2013) 491.

[17] H. Sun, G. Sun, S. Wang, J. Liu, X. Zhao, G. Wang, H. Xu, S. Hou, Q. Xin, J. Membr. Sci. 259 (2005) 27.
[18] J. Zang, C. Li, S. Bao, X. Cui, Q. Bao, C. Sun, Macromolecules 41 (2008) 7053.
[19] C. Debiemme-Chouvy, Electrochem. Commun. 11 (2009) 298.
[20] Y. Ma, J. Zhang, G. Zhang, H. He, J. Am. Chem. Soc. 126 (2004) 7097.
[21] V. Bocharova, A. Kiriy, H. Vinzelberg, I. Mőnch, M. Stamm, Angew. Chem. Int. Ed. 44 (2005) 6391.
[22] D.A. Kaplin, S. Qutubuddin, Polymer 36 (1995) 1275.
[23] J. Huang, K. Wang, Z. Wei, J. Mater. Chem. 20 (2010) 1117.
[24] S. Sadki, P. Schottland, N. Brodiec, G. Sabouraud, Chem. Soc. Rev. 29 (2000) 283.
[25] J.A.V. Butler, Trans. Faraday Soc. 19 (1924) 729.
[26] T. Erdey-Gruz, M. Volmer, Z. Phys. Chem. 150A (1930) 203.
[27] A.J. Bard, L.R. Faulkner, Electrochemical Methods: Fundamentals and Applications, Wiley, NJ, USA, 2001.
[28] W. Zhong, S. Liu, X. Chen, Y. Wang, W. Yang, Macromolecules 39 (2006) 3224.
[29] C.D. Paulse, P.G. Pickup, J. Phys. Chem. 92 (1988) 7002.
[30] Y. Yang, M. Wan, J. Mater. Chem. 11 (2001) 2022.
[31] C. Lim, C.Y. Wang, Electrochim. Acta 49 (2004) 4149.
[32] W. Barthlott, C. Neinhuis, Planta 202 (1997) 1.
[33] P. Roach, N.J. Shirtcliffe, M.I. Newton, Soft Matter 4 (2008) 224.
[34] R.N. Wenzel, Ind. Eng. Chem. 28 (1936) 988.
[35] A.B.D. Cassie, S. Baxter, Trans. Faraday Soc. 40 (1944) 546.
[36] A. Pozio, M. De Francesco, A. Cemmi, F. Cardellini, L. Giorgi, J. Power Sources 105 (2002) 13.
[37] M. Prasanna, H.Y. Ha, E.A. Cho, S.A. Hong, I.H. Oh, J. Power Sources 137 (2004) 1.